The Astrophysical Journal Letters, 983:L37 (8pp), 2025 April 20 https://doi.org/10.3847/2041-8213/adc680

The Convergence of Heavy and Light Seeds to Overmassive Black Holes at Cosmic Dawn

Haojie Hu[1,2,3,7], Kohei Inayoshi[2], Zoltán Haiman[4,5,6], Luis C. Ho[2,3], and Ken Ohsuga[1]
[1] Center for Computational Science, University of Tsukuba, 1-1-1 Tennodai, Tsukuba, Ibaraki 305-8577, Japan; huhaojie@ccs.tsukuba.ac.jp
[2] Kavli Institute for Astronomy and Astrophysics, Peking University, 5 Yiheyuan Road, Haidian District, Beijing 100871, People's Republic of China; inayoshi@pku.edu.cn
[3] Department of Astronomy, School of Physics, Peking University, 5 Yiheyuan Road, Haidian District, Beijing 100871, People's Republic of China
[4] Department of Astronomy, Columbia University, New York, NY 10027, USA
[5] Department of Physics, Columbia University, New York, NY 10027, USA
[6] Institute of Science and Technoogy Austria, AM Campus 1, Klosterneuburg 3400, Austria
Received 2025 March 5; revised 2025 March 26; accepted 2025 March 28; published 2025 April 15

Abstract

The James Webb Space Telescope has revealed low-luminosity active galactic nuclei at redshifts of $z \gtrsim 4$–7, many of which host accreting massive black holes (BHs) with BH-to-galaxy mass ($M_{\rm BH}/M_\star$) ratios exceeding the local values by more than an order of magnitude. The origin of these overmassive BHs remains unclear but requires potential contributions from heavy seeds and/or episodes of super-Eddington accretion. We present a growth model coupled with dark matter halo assembly to explore the evolution of the $M_{\rm BH}/M_\star$ ratio under different seeding and feedback scenarios. Given the gas inflow rates in protogalaxies, BHs grow episodically at moderate super-Eddington rates, and the mass ratio increases early on, despite significant mass loss through feedback. Regardless of seeding mechanisms, the mass ratio converges to a universal value ∼0.1–0.3, set by the balance between gas feeding and star formation efficiency in the nucleus. This behavior defines an attractor in the $M_{\rm BH}$–$M_\star$ diagram, where overmassive BHs grow more slowly than their hosts, while undermassive seeds experience rapid growth before aligning with the attractor. We derive an analytical expression for the universal mass ratio, linking it to feedback strength and halo growth. The convergence of evolutionary tracks erases seeding information from the mass ratio by $z \sim 4$–6. Detecting BHs with $\sim 10^{5-6}\,M_\odot$ at higher redshifts that deviate from the convergence trend would provide key diagnostics of their birth conditions.

Unified Astronomy Thesaurus concepts: Supermassive black holes (1663); Quasars (1319); High-redshift galaxies (734); Active galactic nuclei (16); Scaling relations (2031)

1. Introduction

The James Webb Space Telescope (JWST) with its exceptional sensitivity has enabled the discovery of faint active galactic nuclei (AGNs) in the high-redshift Universe ($z > 4$–7, e.g., M. Onoue et al. 2023; D. D. Kocevski et al. 2024), pushing the detection limits of AGN luminosities to $L_{\rm bol} \sim 10^{45}$ erg s^{-1} and black hole (BH) masses to $M_{\rm BH} \sim 10^6\,M_\odot$ (e.g., Y. Harikane et al. 2023; R. Maiolino et al. 2024a). A significant fraction of these newly discovered AGNs host supermassive BHs (SMBHs) with BH-to-host galaxy mass ratios reaching values of $M_{\rm BH}/M_\star \gtrsim 0.01$–0.1 (C.-H. Chen et al. 2024), significantly higher than the empirical value ($\lesssim$0.01) observed in the present-day Universe by more than an order of magnitude (e.g., J. Kormendy & L. C. Ho 2013; A. E. Reines & M. Volonteri 2015). While such overmassive BHs were previously identified in rare, ultraluminous quasars (D. J. Mortlock et al. 2011; X.-B. Wu et al. 2015; E. Bañados et al. 2018; X. Fan et al. 2023; also local overmassive SMBHs, e.g., R. C. E. van den Bosch et al. 2012), JWST has now revealed similar trends in fainter, more representative AGN populations, providing strong constraints on the early stages of BH–galaxy coevolution as well as the assembly process of each component (e.g., A. Trinca et al. 2022; W. Li et al. 2024; J. Li et al. 2025).

The rapid assembly of SMBHs in the first billion years of the Universe has been extensively debated (e.g., K. Inayoshi et al. 2020; M. Volonteri et al. 2021 and references therein). Two main scenarios have been proposed: (1) rapid gas accretion of stellar remnant BHs at or above the Eddington rate with a high duty cycle from early epochs at $z \gtrsim 20$ (Z. Haiman & A. Loeb 2001; P. Madau & M. J. Rees 2001; M. Volonteri et al. 2003), and (2) moderate growth from more massive seed BHs formed via direct collapse of massive primordial gas clouds or runaway stellar collisions in dense environments (e.g., S. P. Oh & Z. Haiman 2002; V. Bromm & A. Loeb 2003; M. C. Begelman et al. 2006; G. Lodato & P. Natarajan 2006; K. Omukai et al. 2008; J. A. Regan & M. G. Haehnelt 2009a, 2009b; H. Tagawa et al. 2020; W. Li et al. 2023). These mechanisms are widely considered essential for explaining the high BH-to-stellar mass ratio observed in JWST-identified AGNs (e.g., H. Hu et al. 2022; K. Inayoshi et al. 2022; M. T. Scoggins & Z. Haiman 2024). While some extreme cases may originate from massive seed BHs, which naturally yield high BH-to-galaxy mass ratios at birth (e.g., UHZ1, an AGN candidate with $M_{\rm BH}/M_\star \simeq 1.0$; Á. Bogdán et al. 2024), possibly originating from a DCBH (P. Natarajan et al. 2024), intermittent super-Eddington accretion could also drive even light seed BHs to outgrow their hosts if sustained gas inflows are available (H. Hu et al. 2022; K. Inayoshi et al. 2022; M. T. Scoggins & Z. Haiman 2024). Despite both pathways being plausible, a key challenge

[7] Japan Society for the Promotion of Science (JSPF) fellow.

is understanding how BH–host interactions shape their long-term evolutionary trajectories.

AGN and stellar feedback play a central role in regulating BH growth (J. Jeon et al. 2023, 2025). However, most cosmological galaxy-formation simulations, which rely on subgrid feedback models due to limited spatial resolution, predict substantially lower $M_{\rm BH}/M_\star$ ratios than those observed, i.e., undermassive BHs. According to these models, galaxies grow first through star formation, while BH growth is delayed until galaxies become massive enough to retain gas in the nuclei due to their deeper gravitational potential wells (Y. Dubois et al. 2015; D. Anglés-Alcázar et al. 2017; M. Habouzit et al. 2017; M. Habouzit 2025). This tension between these simulation results and the JWST-identified AGNs/BHs with high $M_{\rm BH}/M_\star$ ratios highlights the need for a revised treatment of feedback processes in galactic nuclei at early times.

In this Letter, we present a BH growth model coupled with DM halo assembly to explore the emergence of overmassive BH populations with $M_{\rm BH}/M_\star > 0.01$, exceeding the values observed in the local Universe. We parameterize feedback-driven mass loss by modeling gas inflow rates toward the nucleus as a power-law function, $\dot{M}(r) \propto r^p$, where p encapsulates uncertainties of feedback effects. By incorporating BH and galaxy growth rates tied to DM halo evolution, we develop a semianalytical framework to map evolutionary trajectories in the $M_{\rm BH}$–$M_\star$ diagram. The model successfully reproduces the $M_{\rm BH}$–$M_\star$ distribution of JWST-identified AGNs and BHs at $z \sim 4$–7 (e.g., V. Kokorev et al. 2023; Á. Bogdán et al. 2024; J. E. Greene et al. 2024) across different seeding channels, even with significant mass loss through feedback. We further discuss how rapid assembly processes diminish seeding information from $M_{\rm BH}/M_\star$ ratios of observed AGN populations. Throughout this Letter, we assume a flat Λ cold dark-matter universe with the following cosmological parameters: $h = 0.6732$, $\Omega_{\rm m} = 0.3158$, and $\sigma_8 = 0.8120$ (Planck Collaboration et al. 2020).

2. The Early Growth of Seed BH and Evolution of the $M_{\rm BH}/M_\star$ Ratio

In this study, we construct an analytical framework to model the mass growth of BHs and their host galaxies. In the hierarchical structure formation paradigm, we link the rate of baryon inflow into the galactic nucleus to the DM halo mass assembly as

$$\dot{M}_0 = \epsilon_{\rm nuc} f_{\rm b} \frac{dM_{\rm halo}(t)}{dt}, \quad (1)$$

where $f_{\rm b} = 0.16$ is the baryonic fraction (Planck Collaboration et al. 2020) and $\mathrm{d}M_{\rm halo}/\mathrm{d}t$ is the DM halo growth rate obtained through a Monte Carlo merger tree algorithm (H. Parkinson et al. 2008; W. Li et al. 2021). Generally, incoming gas from the parent halo is assembled into a galactic disk and then consumed either by star formation or BH accretion, or possibly ejected into galactic outflows (J. W. Wadsley et al. 2004; F. Fraternali et al. 2005; F. Fraternali & J. J. Binney 2006; T. Kaufmann et al. 2006). We assume that a fraction $\epsilon_{\rm nuc}$ of the gas inflow feeds the nuclear region and set a fiducial value of $\epsilon_{\rm nuc} = 0.1$ based on the results obtained by cosmological hydrodynamic simulations resolving multiscales down to $\sim$0.1 pc (P. F. Hopkins & E. Quataert 2010).

We assume the BH accretion rate to match the nuclear gas supply rate, i.e., $\dot{M}_{\rm BH} = \dot{M}_0$, when it is below the Eddington limit. In contrast, when the inflow rate exceeds this limit, we consider mass removal via radiation-driven outflows to reduce the BH feeding rate as (H. Hu et al. 2022)

$$\dot{M}_{\rm BH} = \dot{M}_0 \times \min\left\{1, \left(\frac{r_{\rm in}}{r_{\rm out}}\right)^p\right\}, \quad (2)$$

where $r_{\rm in}$ and $r_{\rm out}$ are the inner and outer radii, where the gas inflow rate decreases toward the center. The power-law index of p characterizes the outflow strength and the efficiency of mass removal by outflows. The index is measured as $p \simeq 0.5$ for super-Eddington accretion cases (H. Hu et al. 2022), but it ranges over $0 < p < 1$ in more general situations (see F. Yuan & R. Narayan 2014). In this work, we set $r_{\rm in}$ to the innermost stable circular orbit radius and $r_{\rm out}$ to the photon-trapping radius in the accretion flow, i.e., $r_{\rm in} = 6GM_{\rm BH}/c^2$ and $r_{\rm out} = \kappa_{\rm T}\dot{M}_0/(4\pi c)$, with G the gravitational constant, c the speed of light, and $\kappa_{\rm T}$ the electron scattering opacity. The transition due to outflows occurs when $\dot{m}_0 (\equiv \dot{M}_0/\dot{M}_{\rm Edd})$ exceeds 0.6, where the Eddington accretion rate is defined as $\dot{M}_{\rm Edd} \equiv L_{\rm Edd}/(0.1c^2)$ and $L_{\rm Edd}$ is the Eddington luminosity. As a result, the BH accretion rate in Equation (2) is rewritten as

$$\dot{M}_{\rm BH} = \dot{M}_0 \times \min\left\{1, \left(\frac{\dot{m}_0}{0.6}\right)^{-p}\right\}. \quad (3)$$

To quantify the stellar mass evolution in a galaxy, we assume a star formation efficiency (SFE) $\epsilon_\star$, where the star formation rate is given by $\dot{M}_\star = \epsilon_\star \dot{M}_0/\epsilon_{\rm nuc}$. We here only consider a high and constant SFE model ($\epsilon_\star = 0.5$), which is motivated by JWST observations of UV bright galaxies at $z > 10$, whose SFEs are expected to be as high as $\sim$0.3–0.5 (e.g., K. Inayoshi et al. 2022; K. M. Pontoppidan et al. 2022; Y.-Y. Wang et al. 2023). This model provides a higher stellar mass for a given inflow rate and thus lower $M_{\rm BH}/M_\star$ ratios, compared to those assumed in previous semianalytical studies (e.g., P. Behroozi et al. 2019; M. T. Scoggins & Z. Haiman 2024).

In the left panel of Figure 1, we present evolutionary tracks for DM halo mergers and BHs, along with distribution of high-redshift quasars observed with JWST (black crosses; X. Ding et al. 2023; Y. Harikane et al. 2023; D. D. Kocevski et al. 2023, 2024; V. Kokorev et al. 2023; R. L. Larson et al. 2023; R. Maiolino et al. 2024a, 2024b; M. Yue et al. 2023; Á. Bogdán et al. 2024; J. E. Greene et al. 2024; I. Juodžbalis et al. 2024; M. A. Stone et al. 2024) and with other surveys (gray crosses; D. J. Mortlock et al. 2011; X.-B. Wu et al. 2015; E. Bañados et al. 2018; T. Izumi et al. 2019). The gray solid curves are evolutionary tracks of the main DM halo progenitors that end up in massive halos with $M_{\rm h} = 10^{12}\,M_\odot$ at $z = 6$ (W. Li et al. 2021), the characteristic halo predicted by the Press–Schechter formalism, when comparing the growth rate of quasar density to observations (J. S. B. Wyithe & T. Padmanabhan 2006). As examples, we highlight three representative merger trees (black curves) and the corresponding mass evolution of BHs originating from two BH seeding scenarios that are initiated and grow within these

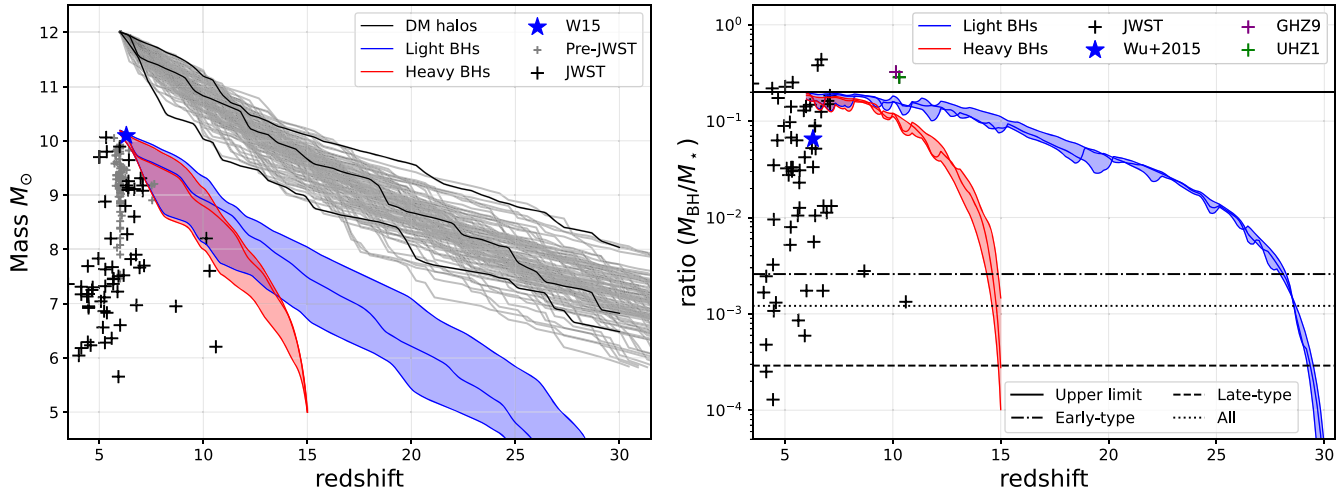

Figure 1. Left: the mass evolution for DM mergers and seed BHs. The gray curves are evolutionary tracks of main progenitors of 100 (out of 10^4) DM halos ended up as massive halos with $M_{\rm h} = 10^{12}\,M_\odot$ at $z = 6$. Three typical merger histories are shown in black solid curves. The growth rate ($k_{\rm h}$) for different merger trees at $z \sim 6$ varies from ∼0.25 to ∼1.15. The blue and red curves are evolutionary tracks for light ($10\,M_\odot$ BH at $z = 30$) and heavy seed ($10^5\,M_\odot$ at $z = 15$) BHs based on the three merger trees, adopting a fiducial model with $p = 0.5$. The blue and red shaded regions are parameters for possible SMBHs from our models. The high-redshift SMBHs are overlaid with crosses, with the most massive SMBH from X.-B. Wu et al. (2015). SMBHs from the pre-JWST era are overlaid with gray crosses (D. J. Mortlock et al. 2011; E. Bañados et al. 2018; T. Izumi et al. 2019), while SMBHs from the JWST era are shown with black crosses (data collected from X. Ding et al. 2023; Y. Harikane et al. 2023; D. D. Kocevski et al. 2023, 2024; V. Kokorev et al. 2023, 2024; R. L. Larson et al. 2023; R. Maiolino et al. 2024a, 2024b; M. Yue et al. 2023; Á. Bogdán et al. 2024; J. E. Greene et al. 2024; I. Juodžbalis et al. 2024; L. Napolitano et al. 2024; M. A. Stone et al. 2024). Right: the evolution of the $M_{\rm BH}/M_\star$ ratio for light seed BHs (blue curves) and heavy seed BHs (red curves). The JWST samples are overlaid for reference. The solid horizontal line indicates the maximum value of $M_{\rm BH}/M_\star \sim \epsilon_{\rm nuc}/\epsilon_\star = 0.2$. The dashed, dashed–dotted, and dotted horizontal lines are $M_{\rm BH}/M_\star$ ratios for late-type, early-type, and all galaxies at $M_\star = 3 \times 10^{10}\,M_\odot$, respectively (J. E. Greene et al. 2020).

representative halos. The light seed BHs (blue curves) are originated from Population III stellar remnants at $z = 30$ with $M_{\rm BH} = 10\,M_\odot$, while the heavy seed BHs (red curves) begin their mass growth at $z = 15$ with initial masses of $M_{\rm BH} = 10^5\,M_\odot$.[8] Both types of seed BHs undergo early rapid growth phases, and all tracks reach $M_{\rm BH} \simeq 10^{10}\,M_\odot$ by $z \sim 6$. The BH mass and redshift are consistent with those of the brightest quasars at $z \sim 6$ (X.-B. Wu et al. 2015).

In the right panel of Figure 1, we show the evolution of the $M_{\rm BH}/M_\star$ ratio as a function of redshift for the two BH seeding scenarios in the three DM halo trees. In both cases, the ratio increases rapidly during the early stage and overshoots the empirical value observed in the local Universe. Although the galaxy gains stellar mass efficiently with a high SFE ($\epsilon_\star = 0.5$), the rapid growth of BHs drives the ratio to $M_{\rm BH}/M_\star \sim 0.1$ by $z \sim 6$, consistent with observations of overmassive SMBHs (e.g., Y. Harikane et al. 2023; Á. Bogdán et al. 2024; R. Maiolino et al. 2024a;). It is worth noting that the final mass ratio is determined by the last accretion episodes at $z \sim 6$, when the growth rate transitions to a sub-Eddington value. In the sub-Eddington regime, all inflowing gas is assumed to feed the central BH without significant mass loss, naturally leading to $M_{\rm BH}/M_\star \simeq \epsilon_{\rm nuc}/\epsilon_\star (=0.2)$. We note that the mass ratio might be reduced if the AGN feedback operates even in the sub-Eddington regime, where we currently set $p = 0$ in this model.

In this framework, the rapid growth phases of seed BHs make the distinction between seeding scenarios challenging. Both light and heavy seed BHs converge in their evolutionary tracks by $z \lesssim 10$, making the $M_{\rm BH}/M_\star$ ratio an inefficient discriminator of seeding models. Therefore, observing the early evolutionary stages of less massive BHs may help break the degeneracy.

3. Global Flow Structure on the $M_{\rm BH}$–$M_\star$ Diagram

3.1. Analytical Formulation

In the previous section, we developed evolutionary tracks for different seed BHs along specific halo assembly histories and investigated the evolution of the $M_{\rm BH}/M_\star$ ratio to account for the presence of luminous quasars at $z \sim 6$. In this section, we extend our analysis to explore the broader evolutionary trends of $M_{\rm BH}/M_\star$ ratios across a wider range of parameters. Specifically, we examine the patterns in the $M_{\rm BH}$–$M_\star$ diagram for the entire BH population, including the less luminous and less massive BHs recently uncovered by JWST observations (e.g., Y. Harikane et al. 2023; D. D. Kocevski et al. 2023; R. Maiolino et al. 2024a).

To achieve this, we generalize the halo assembly tracks and extend the model to cover a broader parameter space. This allows us to explore the $M_{\rm BH}/M_\star$ ratio for SMBHs of varying masses in different galaxies, using the following analytical formula:

$$M_{\rm halo}(z) = \mathcal{M} \cdot \exp(-k_{\rm h} z), \tag{4}$$

where $\mathcal{M}$ is the mass normalization and $k_{\rm h}$ represents the growth rate of the DM halo. This redshift dependence arises from the Press–Schechter formalism (W. H. Press & P. Schechter 1974; C. Lacey & S. Cole 1993; S. Cole et al. 2000) and aligns with fits to merger trees from cosmological N-body simulations (O. Fakhouri et al. 2010; A. Dekel et al. 2013), yielding the mass growth rate of $d \ln M_{\rm h}/dt \propto k_{\rm h}(1+z)^{5/2}$. The mean value of $k_{\rm h}$ for all merger trees is estimated from comparison to these

[8] When a heavy BH is seeded at $z = 15$, the initial $M_{\rm BH}/M_\star$ ratio is $\leqslant 3 \times 10^{-4}$. This value is lower than the empirical values observed in the local Universe as well as the typical ratio expected for newly born heavy seed BHs through either direct collapse of massive gas clouds or stellar dynamical processes (e.g., M. A. Gürkan et al. 2004; B. Agarwal et al. 2013; K. Inayoshi et al. 2018). In Section 3.3, we will discuss the evolution of heavy seeds with high initial $M_{\rm BH}/M_\star$ ratios motivated by these theoretical models.

simulations (e.g., O. Fakhouri et al. 2010) as $\langle k_{\rm h}\rangle \simeq 0.7$. For halos reaching $M_{\rm halo} = 10^{12}\,M_\odot$ at $z = 6$, the power-law index ranges over $0.25 \lesssim k_{\rm h} \lesssim 1.15$, as illustrated by the three representative merger trees in Figure 1.

Using this functional form for stellar mass growth with an SFE of $\epsilon_\star$, the ratio of $\dot{M}_{\rm BH}/\dot{M}_\star$ is calculated as

$$\frac{\dot{M}_{\rm BH}}{\dot{M}_\star} = \frac{dM_{\rm BH}}{dM_\star} = C_p(z)\left(\frac{M_{\rm BH}}{M_\star}\right)^p, \tag{5}$$

and

$$C_p(z) = \left(\frac{t_{\rm Edd}}{t_\star}\right)^{-p}\left(\frac{\epsilon_{\rm nuc}}{\epsilon_\star}\right)^{1-p}, \tag{6}$$

where $t_{\rm Edd} \simeq 45\,{\rm Myr}$ is the e-folding timescale for the Eddington-limited growth with a 10% radiative efficiency, and the characteristic star formation timescale $t_\star$ is defined as

$$t_\star = \frac{3}{5H_0(1+z)E(z)k_{\rm h}} \simeq 49\,{\rm Myr}\quad k_{\rm h}^{-1}\left(\frac{1+z}{10}\right)^{-5/2}, \tag{7}$$

where $E(z) = [(1+z)^3\Omega_{\rm m} + \Omega_\Lambda]^{1/2}$ and $z > (\Omega_\Lambda/\Omega_{\rm m})^{1/3} - 1 \simeq 0.3$ are considered. Therefore, for given values of initial $M_{\rm BH}/M_\star$, p, $k_{\rm h}$, and z, one can numerically calculate the ratio of the growth rates of the BH and stellar masses and draw the "velocity" vectors on the $M_\star$–$M_{\rm BH}$ diagram.

The behavior of the evolutionary track can be understood in a simple way because the numerical factor $C_p(z)$ evolves slowly with redshift compared to the stellar mass growth, as described by

$$\frac{d\ln C_p}{d\ln M_\star} = \frac{5p/2}{k_{\rm h}(1+z)} \simeq 0.16, \tag{8}$$

for $p = 0.5$, $k_{\rm h} = 0.7$, and $z = 10$. Thus, when C_p is approximated as a constant value (due to a small p-value or high redshift), the mass ratio $M_{\rm BH}/M_\star$ asymptotically approaches

$$\frac{M_{\rm BH}}{M_\star} \;\rightarrow\; C_p^{\frac{1}{1-p}}, \tag{9}$$

regardless of the p-value in the limit of weak or moderate feedback ($p \lesssim 0.5$). In this regime, the logarithmic gradient approaches unity as

$$\frac{d\ln M_{\rm BH}}{d\ln M_\star} = C_p\left(\frac{M_{\rm BH}}{M_\star}\right)^{p-1} \rightarrow 1. \tag{10}$$

This asymptotic behavior explains the flow pattern and convergence shown in Figure 2.

Figure 2 illustrates the evolutionary trend of the BH-to-stellar mass ratio at four different redshifts: $z = 25$, 15, 10, and 8. As a reference, the local relation from J. Kormendy & L. C. Ho (2013) is overlaid with the black diagonal line. We adopt a constant value $p = 0.5$ and halo growth rates $k_{\rm h} = 0.7$ at $z \leqslant 15$ and $k_{\rm h} = 0.35$ at $z > 15$ to be consistent with the evolutionary tracks shown in Figure 1. The arrows indicate the evolutionary direction for the given boundary conditions, i.e., BH mass, halo growth, and feedback strength. Their lengths are calculated based on the growth of BH mass and stellar masses over the next 10 Myr and renormalized to [0.2, 1.2] times the length of a unit vector for visualization. The two-dimensional plane is divided into two regions based on the gradient of the vector field (i.e., acceleration in the analogy of fluid dynamics), $\mathscr{S} \equiv d^2\ln M_{\rm BH}/(d\ln M_\star)^2$: the region with blue arrows where $\mathscr{S} > 0$ and region with gray arrows where $\mathscr{S} < 0$, respectively. The boundary where $\mathscr{S} = 0$ is shown as a diagonal orange line in the $M_{\rm BH}$–$M_\star$ diagram, as derived in Equation (10). Below the boundary of $\mathscr{S} = 0$, the BH mass tends to grow faster than the stellar mass and approaches the boundary. On the other hand, above the boundary, the stellar mass grows faster than the BH mass and approaches the boundary. In both cases, the boundary of $\mathscr{S} = 0$ becomes an attractor, and the mass ratio approaches a constant value given by Equation (9).

As examples, we overlay the evolutionary tracks of two types of seed BHs: a light seed BH with an initial mass of $M_{\rm BH} = 10\,M_\odot$ at $z = 30$ and a heavy seed BH with $M_{\rm BH} = 10^5\,M_\odot$ at $z = 15$. Each track features an open circle representing the transition from super-Eddington accretion regime to sub-Eddington regime. The solid curves illustrate the evolution from the seeding phase to that redshift, while the dashed curves indicate the continuation of the tracks toward lower redshifts. Initially, the two cases have BHs undermassive relative to their host galaxies and lie below the local relation (J. Kormendy & L. C. Ho 2013), with $\mathscr{S} < 0$. Given the fiducial feedback strength ($p = 0.5$), these seed BHs experience rapid but decelerating growth during their early evolutionary stages. This initial rapid growth increases the $M_{\rm BH}/M_\star$ ratio to values significantly above the local relationship. After that, the two evolutionary tracks nearly converge to a similar locus by $z \simeq 6$, making it difficult to distinguish between the BH seeding models based on the observed mass ratio at $z \lesssim 6$. The converging mass ratio is primarily determined by the feedback strength p (see also Equation (9)). However, as the gas supply rate to the galactic nucleus transitions to the sub-Eddington regime (evolutionary tracks after open circles; $p = 0$ is assumed in the feedback prescription) at lower redshifts, the final mass ratio approaches $M_{\rm BH}/M_\star = \epsilon_{\rm nuc}/\epsilon_\star (\simeq 0.2)$. We caution that the realistic inflow rate is expected to be more stochastic, episodically transitioning between super-Eddington and sub-Eddington regimes. However, this model smooths out such variability, resulting in a gradual transition from the super-Eddington to the sub-Eddington regime in the final stages.

3.2. The Variation due to Feedback Models

While radiation hydrodynamic simulations that focus on accretion flows at the vicinity of a BH event horizon suggest that the power-law index of the inflow rate profile generally falls within $p \simeq 0.5$–0.7 (e.g., F. Yuan & R. Narayan 2014; H. Hu et al. 2022), realistic feedback processes are more complex and have significant influences on both BH accretion and gas supply from galactic scales. Cosmological galaxy-formation simulations indicate that the efficiency of gas removal due to feedback is closely linked to the host stellar mass (e.g., A. J. Benson 2010; P. F. Hopkins et al. 2012; B. W. Keller et al. 2015; R. S. Somerville & R. Davé 2015; L. Mayer et al. 2016; A. Oklopčić et al. 2017; R. Weinberger et al. 2017; J.-h. Kim et al. 2019; Y. Qin et al. 2019; A. Chakraborty et al. 2023). In low-mass galaxies, AGN activity and supernova explosions in their shallow gravitational potential efficiently evacuate gas from the nucleus, strongly suppressing BH accretion. In contrast, in higher-mass galaxies, the deeper gravitational potential retains gas, reducing the

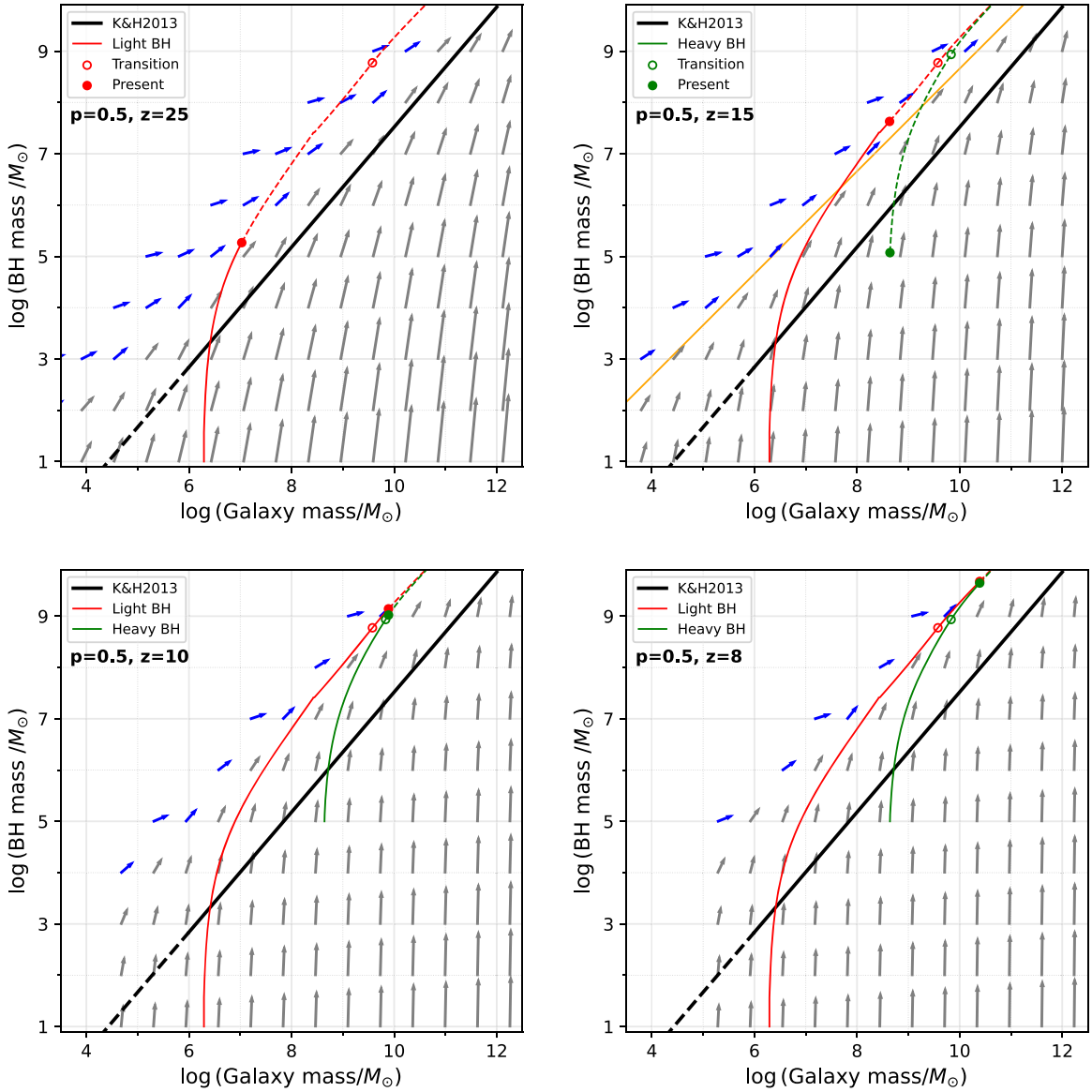

Figure 2. The evolutionary trend for two different seed BHs at four epochs ($z = 25$, 15, 10, and 8). The blue (gray) arrows indicate positive (negative) second-order derivatives $\mathscr{S}$, while lengths of arrows are calculated assuming a 10 Myr growth for the BH and host galaxy at the current epoch and renormalized to [0.2, 1.2] times the length of a unit vector. The two evolutionary tracks represent that for a light seed with an initial mass of $M_{\rm BH} = 10\,M_\odot$ at $z = 30$ (red) and a heavy seed with $M_{\rm BH} = 10^5\,M_\odot$ at $z = 15$ (green). The solid curve illustrates the evolution from the seeding time to the redshift of each panel (marked with filled circles), while the dashed curves show the continuation of the track toward lower redshifts. In this figure, we adopt a constant value $p = 0.5$ and halo growth rates $k_{\rm h} = 0.7$ at $z \leqslant 15$ and $k_{\rm h} = 0.35$ at $z > 15$ to be consistent with the evolutionary tracks shown in Figure 1. The open circle in each model indicates the transition from super-Eddington to sub-Eddington accretion, after which $p = 0$ is assumed. The diagonal orange line in the top right panel represents the boundary with $\mathscr{S} = 0$ for $p = 0.5$.

impact of feedback and allowing BHs to accrete more efficiently. Given this mass dependence, modeling the evolution of the $M_{\rm BH}/M_\star$ ratio under different feedback strengths is crucial for understanding the BH–galaxy coevolution.

To capture this mass dependence, we introduce a critical stellar mass at which feedback strength varies due to the deepening gravitational potential of galaxies. Motivated by cosmological galaxy-formation simulation results, we parameterize the stellar-mass-dependent feedback model using a hyperbolic tangent function,

$$p = p_0 - \delta p \cdot \tanh x, \tag{11}$$

where $x = 1.5 \cdot \log_{10}(M_\star/M_{\rm p})$ and $M_{\rm p}$ represents the transition mass where feedback strength changes significantly. Due to the complexity of cosmological simulations, neither the transition mass nor the feedback strengths for different modes are well constrained. We thus adopt the following parameter sets (shown as inserts in Figure 3): (1) SP1 (stellar-mass-dependent p model, SP): the transition between strong and moderate feedback occurs at $M_{\rm p} = 10^7\,M_\odot$ with $p_0 = 0.75$ and $\delta p = 0.25$; (2) SP2: the feedback strengths (p_0 and δp) are the same as in SP1, but the transition mass is set at $M_{\rm p} = 10^9\,M_\odot$; and (3) SP3: the transition occurs at $M_{\rm p} = 10^9\,M_\odot$, but strong feedback persists to some extent after the transition, with $p_0 = 0.875$ and $\delta p = 0.125$.

In Figure 3, we demonstrate the evolutionary trends of BHs and host galaxies at $z = 15$ for these stellar-mass dependent feedback models. The overall evolutionary patterns resemble those seen in the constant feedback model in Figure 2. Overmassive BHs (relative to the boundary line) grow slowly,

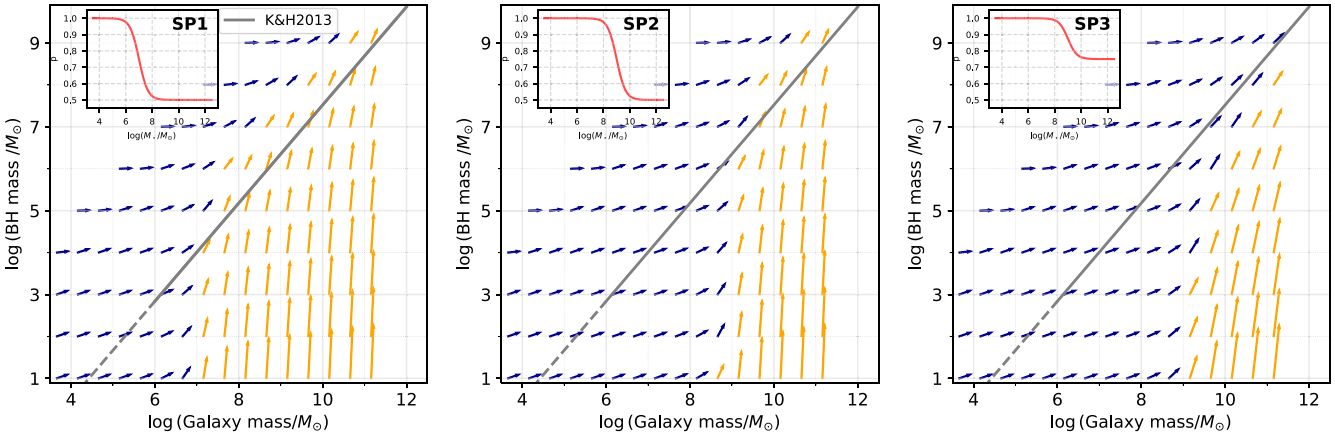

Figure 3. The evolutionary trend for different feedback models at $z = 15$ (from left to right: SP1, SP2, and SP3). The blue arrows indicate the positive signs of second-order derivatives, while the orange arrows are for negative ones. The lengths of arrows are same as in Figure 2. The inserts in each panel show the corresponding feedback models.

approaching the boundary, while undermassive BHs grow rapidly toward it. At low masses, strong feedback significantly suppresses early BH growth. As the host galaxies evolve, weakened feedback allows their central BHs to grow more efficiently, as consistently observed in most cosmological simulations. As in the constant feedback models, the evolutionary trajectories tend to converge toward the $\mathscr{S} = 0$ boundary curves, making them attractors for BH–galaxy coevolution. However, in stellar-mass-dependent feedback models, the boundary curve shapes differ. The transition between different feedback strengths at the characteristic mass scale $M_{\rm p}$ defines a distinct twisted point on the boundary lines. At higher masses, the final convergent points are determined by the feedback strength at $M_\star > M_p$. This figure indicates that a weak feedback strength as low as $p = 0.5$ is sufficient to account for most of the overmassive BHs observed by JWST, while stronger feedback ($p \sim 0.7$–0.8) is required to regulate the $M_{\rm BH}/M_\star$ ratios near the local relation.

3.3. How Long Does Seeding Information Remain?

Following the evolutionary trends outlined in the previous section, the BH population with high $M_{\rm BH}/M_\star$ ratios can be explained by moderate feedback strength during growth. However, the convergence of these evolutionary trends complicates the interpretation of BH seeding models. To address this, we examine the evolutionary tracks for different seeding models in Figure 4, assuming the SP1 feedback model and normal distributions for $k_{\rm h}$ and $\log \epsilon_{\rm nuc}$. The means and dispersions are set to $\langle k_{\rm h}\rangle = 0.70$, $\sigma_k^2 = 0.06$, and $\langle \epsilon_{\rm nuc}\rangle = 0.02$, $\sigma_{\rm nuc}^2 = 0.25$, respectively (note that the evolutionary pattern is drawn using the mean values). We consider two seed models (heavy and light seeds), whose initial BH and galaxy masses at $z = 20$ are shown with the shaded regions in the top left panel of Figure 4. Each seed population evolves according to the evolutionary pattern of the SP1 model. The mass distributions at $z = 15$, 10, 6, and 4 are shown with colored contours, where darker colors indicate higher probability densities (16% and 84%). For reference, the JWST-observed $M_{\rm BH}$–$M_\star$ data at each redshift are overlaid with star symbols.

In Figure 4, we find that, despite significant differences in seed BH masses, a subset of seed BHs from both models grow into the observed overmassive SMBHs at $z \sim 10$. By $z \sim 6$–4, all seed BH populations converge toward the boundary line as expected from the global evolutionary trend. When the convergence is well established, both seed BH models account for the entire distribution of overmassive SMBHs at $z \sim 6$. However, the growth of most heavy seed BHs appears stunted, clustering around the characteristic mass scale $M_{\rm p} = 10^7\,M_\odot$.

Our model suggests that both light and heavy seed BHs can produce overmassive SMBHs through a convergent evolutionary path. This implies that the only way to distinguish the origins of seed BHs is to trace their early evolution before they reach convergence ($z \gtrsim 6$–10). Specifically, detecting BHs with masses of $\sim 10^{5-6}\,M_\odot$ at higher redshifts that deviate from the linear relation set by the convergence phase would provide a key diagnostic, as their birth conditions remain imprinted at that stage. The question of how long overly massive DCBH seeds remain significant outliers in the $M_{\rm BH}$–$M_\star$ relations has been recently explored using the Renaissance simulations (M. T. Scoggins et al. 2023), semianalytic models (M. T. Scoggins & Z. Haiman 2024), and recent JWST data on 50 broad-line AGNs within the redshift range $3.5 < z < 6.8$ (A. J. Taylor et al. 2024). These studies conclude that, while such seeds remain well above the local scaling relations for several hundred million years, they likely "lose" the memory of their birth by redshifts as low as $z \sim 5$. An illustrative example is the GN-72127 system at $z \sim 4$ (V. Kokorev et al. 2024), which began in the overmassive regime and is now progressing toward the local relation after a recent starburst and subsequent quenching, losing all of its birth information.

4. Summary and Discussions

In this Letter, we present a BH growth model coupled with DM halo assembly to explore the emergence of overmassive BH populations with $M_{\rm BH}/M_\star > 0.01$, exceeding the values observed in the local Universe. We parameterize AGN feedback-driven mass loss as $\dot{M}(r) \propto r^p$ $(0 < p < 1)$, providing a semianalytical framework to map evolutionary trajectories in the $M_{\rm BH}$–$M_\star$ diagram. The growth rates of BHs and galaxies form a converging flow pattern toward a linear attractor set by feedback strength p and gas supply efficiency to the nuclei. Overmassive seed BHs grow more slowly than their hosts, while undermassive seeds experience rapid growth before aligning with the attractor trajectory.

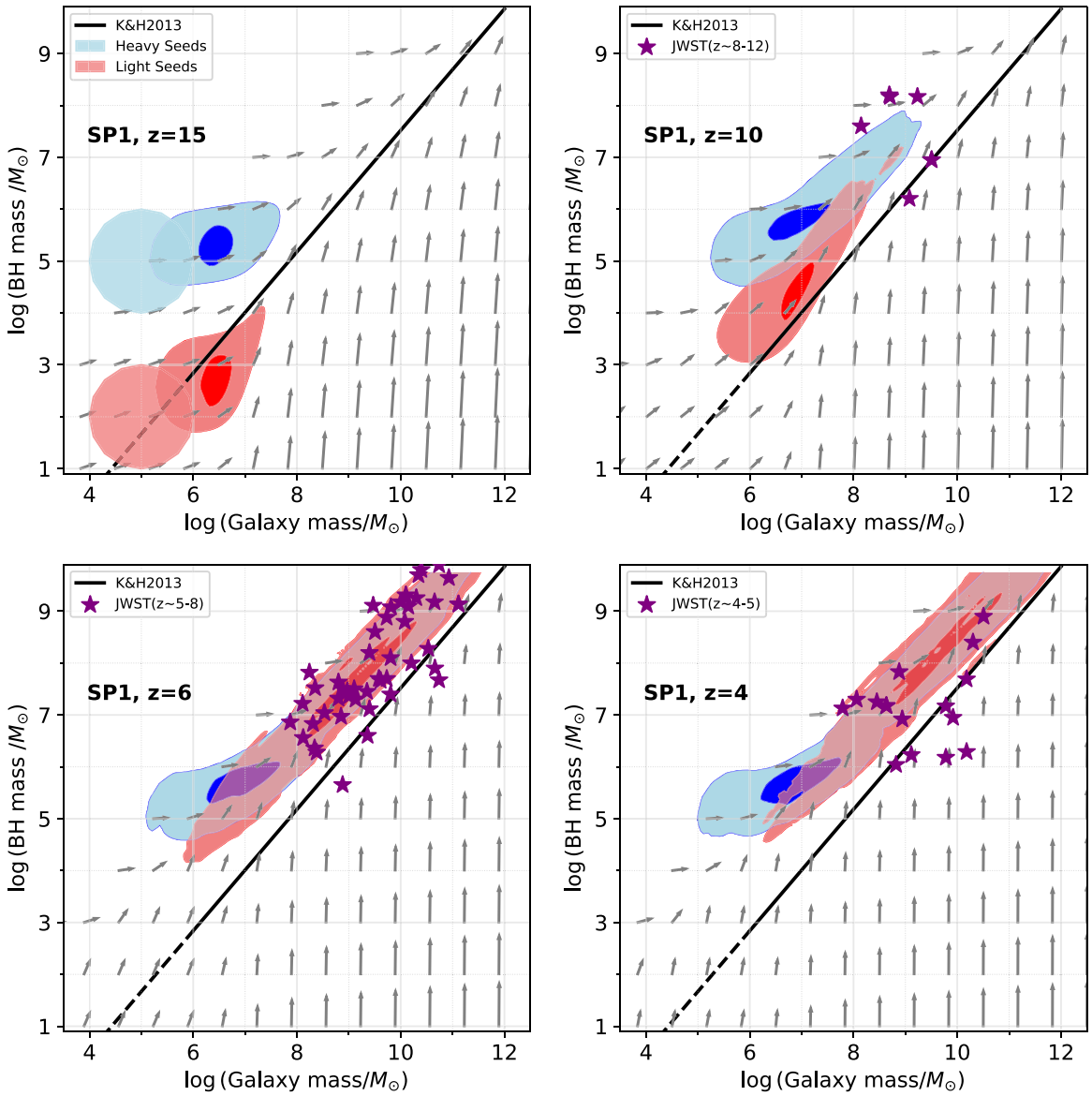

Figure 4. The evolutionary tracks for two classes of seed BHs harbored in galaxies on different mass scales: the blue region for heavy seed BHs and the red region for light seed BHs. The flow patterns are calculated at each redshift adopting the SP1 feedback model. The seed BHs are chosen so that they are located above and below the local relation when they were seeded at $z = 15$. The BH–galaxy systems evolve to $z = 4$ with JWST SMBHs overlaid with stars in each redshift bin. For our fiducial parameters, we adopt $k_{\rm h} = 0.7$ and $\epsilon_{\rm nuc} = 0.02$. The two colored contours are the probability distributions of the evolutionary tracks for the two seed BH models when normal distributions for $k_{\rm h}$ and $\epsilon_{\rm nuc}$ are adopted, with $\langle k_{\rm h}\rangle = 0.70$, $\sigma_k^2 = 0.06$, and $\langle \log \epsilon_{\rm nuc}\rangle = -1.7$, $\sigma_{\rm nuc}^2 = 0.25$. The contour lines represent coverages of 16% and 84%, respectively.

Our model reproduces the $M_{\rm BH}$–$M_\star$ distribution of JWST-identified AGNs and BHs at $z \sim 4$–7 (e.g., V. Kokorev et al. 2023; Á. Bogdán et al. 2024; J. E. Greene et al. 2024) across different seeding channels. However, the convergence behavior erases seeding information from $M_{\rm BH}/M_\star$ ratios observed at $z \sim 4$–6. Detecting BHs $\sim 10^{5-6}\,M_\odot$ at higher redshifts that deviate from the convergence trend would provide key diagnostics of their birth conditions. Meanwhile, we predict a broad distribution of $M_{\rm BH}$–$M_\star$ ratios, some of which might be progenitors for high-z submillimeter galaxies and highly obscured AGNs with undermassive SMBHs. Observations on these populations will constrain and refine our model parameters.

In addition to the broad distribution, M.-Y. Zhuang & L. C. Ho (2023) identified three distinct evolutionary trends for local SMBHs—above, on, and below the $M_{\rm BH}$–$M_\star$ relation. Their analysis suggests that the $M_{\rm BH}/M_\star$ ratio in late-type galaxies gradually converges toward this relation, with overmassive SMBHs experiencing slow growth and undermassive ones growing more rapidly. This evolutionary pattern aligns well with our SP3 model, indicating relatively strong feedback effects in late-type galaxies in the local Universe.

Finally, we caution that despite successfully reproducing the BH–galaxy mass distribution of JWST-identified AGNs at high redshifts, our model is based on simplified prescriptions. The uncertainties in feedback effects are encapsulated in the power-law form of feedback-driven mass loss, whose physical basis derives from numerical simulations and requires further validation through theoretical and observational studies. A more detailed model of high-redshift galaxy formation will be essential to refine the analytical framework presented in this work.

Acknowledgments

We thank the anonymous referee for a careful reading of our manuscript and for comments that helped improve this Letter. This work is supported by the Japan Society for the Promotion of Science (JSPS) KAKENHI grant No. 24KF0130. We acknowledge support from the National Natural Science Foundation of China (12073003, 12003003, 11721303, 11991052, 11950410493), and the China Manned Space Project (CMS-CSST-2021-A04 and CMS-CSST-2021-A06). L.C.H. is supported by the National Science Foundation of China (12233001), the National Key R&D Program of China (2022YFF0503401). Z.H. acknowledges support by US NSF grant AST-2006176 and by NASA grant 80NSSC22K0822. Some of the numerical calculation and analysis were performed with the Cray XC50 at the Center for Computational Astrophysics (CfCA) of the National Astronomical Observatory of Japan and with the High-performance Computing Platform of Peking University.

ORCID iDs

Haojie Hu https://orcid.org/0000-0003-3143-3995
Kohei Inayoshi https://orcid.org/0000-0001-9840-4959
Zoltán Haiman https://orcid.org/0000-0003-3633-5403
Luis C. Ho https://orcid.org/0000-0001-6947-5846
Ken Ohsuga https://orcid.org/0000-0002-2309-3639

References

Agarwal, B., Davis, A. J., Khochfar, S., Natarajan, P., & Dunlop, J. S. 2013, MNRAS, 432, 3438
Anglés-Alcázar, D., Faucher-Giguére, C.-A., Quataert, E., et al. 2017, MNRAS, 472, L109
Bañados, E., Venemans, B. P., Mazzucchelli, C., et al. 2018, Natur, 553, 473
Begelman, M. C., Volonteri, M., & Rees, M. J. 2006, MNRAS, 370, 289
Behroozi, P., Wechsler, R. H., Hearin, A. P., & Conroy, C. 2019, MNRAS, 488, 3143
Benson, A. J. 2010, PhR, 495, 33
Bogdán, Á., Goulding, A. D., Natarajan, P., et al. 2024, NatAs, 8, 126
Bromm, V., & Loeb, A. 2003, ApJ, 596, 34
Chakraborty, A., Chatterjee, S., Lacy, M., et al. 2023, ApJ, 954, 8
Chen, C.-H., Ho, L. C., Li, R., & Zhuang, M.-Y. 2024, arXiv:2411.04446
Cole, S., Lacey, C. G., Baugh, C. M., & Frenk, C. S. 2000, MNRAS, 319, 168
Dekel, A., Zolotov, A., Tweed, D., et al. 2013, MNRAS, 435, 999
Ding, X., Onoue, M., Silverman, J. D., et al. 2023, Natur, 621, 51
Dubois, Y., Volonteri, M., Silk, J., et al. 2015, MNRAS, 452, 1502
Fakhouri, O., Ma, C.-P., & Boylan-Kolchin, M. 2010, MNRAS, 406, 2267
Fan, X., Bañados, E., & Simcoe, R. A. 2023, ARA&A, 61, 373
Fraternali, F., & Binney, J. J. 2006, MNRAS, 366, 449
Fraternali, F., Oosterloo, T. A., Sancisi, R., & Swaters, R. 2005, in ASP Conf. Ser. 331, Extra-Planar Gas, ed. R. Braun (San Francisco, CA: ASP), 239
Greene, J. E., Labbe, I., Goulding, A. D., et al. 2024, ApJ, 964, 39
Greene, J. E., Strader, J., & Ho, L. C. 2020, ARA&A, 58, 257
Gürkan, M. A., Freitag, M., & Rasio, F. A. 2004, ApJ, 604, 632
Habouzit, M. 2025, MNRAS, 537, 2323
Habouzit, M., Volonteri, M., & Dubois, Y. 2017, MNRAS, 468, 3935
Haiman, Z., & Loeb, A. 2001, ApJ, 552, 459
Harikane, Y., Zhang, Y., Nakajima, K., et al. 2023, ApJ, 959, 39
Hopkins, P. F., & Quataert, E. 2010, MNRAS, 407, 1529
Hopkins, P. F., Quataert, E., & Murray, N. 2012, MNRAS, 421, 3522
Hu, H., Inayoshi, K., Haiman, Z., et al. 2022, ApJ, 935, 140
Inayoshi, K., Harikane, Y., Inoue, A. K., Li, W., & Ho, L. C. 2022, ApJL, 938, L10
Inayoshi, K., Li, M., & Haiman, Z. 2018, MNRAS, 479, 4017
Inayoshi, K., Nakatani, R., Toyouchi, D., et al. 2022, ApJ, 927, 237
Inayoshi, K., Visbal, E., & Haiman, Z. 2020, ARA&A, 58, 27
Izumi, T., Onoue, M., Matsuoka, Y., et al. 2019, PASJ, 71, 111
Jeon, J., Bromm, V., Liu, B., & Finkelstein, S. L. 2025, ApJ, 979, 127
Jeon, J., Liu, B., Bromm, V., & Finkelstein, S. L. 2023, MNRAS, 524, 176
Juodžbalis, I., Maiolino, R., Baker, W. M., et al. 2024, Natur, 636, 594
Kaufmann, T., Mayer, L., Wadsley, J., Stadel, J., & Moore, B. 2006, MNRAS, 370, 1612
Keller, B. W., Wadsley, J., & Couchman, H. M. P. 2015, MNRAS, 453, 3499
Kim, J.-h., Wise, J. H., Abel, T., et al. 2019, ApJ, 887, 120
Kocevski, D. D., Finkelstein, S. L., Barro, G., et al. 2024, arXiv:2404.03576
Kocevski, D. D., Onoue, M., Inayoshi, K., et al. 2023, ApJL, 954, L4
Kokorev, V., Chisholm, J., Endsley, R., et al. 2024, ApJ, 975, 178
Kokorev, V., Fujimoto, S., Labbe, I., et al. 2023, ApJL, 957, L7
Kormendy, J., & Ho, L. C. 2013, ARA&A, 51, 511
Lacey, C., & Cole, S. 1993, MNRAS, 262, 627
Larson, R. L., Finkelstein, S. L., Kocevski, D. D., et al. 2023, ApJL, 953, L29
Li, J., Silverman, J. D., Shen, Y., et al. 2025, ApJ, 981, 19
Li, W., Inayoshi, K., Onoue, M., et al. 2024, ApJ, 969, 69
Li, W., Inayoshi, K., Onoue, M., & Toyouchi, D. 2023, ApJ, 950, 85
Li, W., Inayoshi, K., & Qiu, Y. 2021, ApJ, 917, 60
Lodato, G., & Natarajan, P. 2006, MNRAS, 371, 1813
Madau, P., & Rees, M. J. 2001, ApJL, 551, L27
Maiolino, R., Scholtz, J., Curtis-Lake, E., et al. 2024a, A&A, 691, A145
Maiolino, R., Scholtz, J., Witstok, J., et al. 2024b, Natur, 627, 59
Mayer, L., Tamburello, V., Lupi, A., et al. 2016, ApJL, 830, L13
Mortlock, D. J., Warren, S. J., Venemans, B. P., et al. 2011, Natur, 474, 616
Napolitano, L., Castellano, M., Pentericci, L., et al. 2024, arXiv:2410.18763
Natarajan, P., Pacucci, F., Ricarte, A., et al. 2024, ApJL, 960, L1
Oh, S. P., & Haiman, Z. 2002, ApJ, 569, 558
Oklopčić, A., Hopkins, P. F., Feldmann, R., et al. 2017, MNRAS, 465, 952
Omukai, K., Schneider, R., & Haiman, Z. 2008, ApJ, 686, 801
Onoue, M., Inayoshi, K., Ding, X., et al. 2023, ApJL, 942, L17
Parkinson, H., Cole, S., & Helly, J. 2008, MNRAS, 383, 557
Planck Collaboration, Aghanim, N., Akrami, Y., et al. 2020, A&A, 641, A6
Pontoppidan, K. M., Barrientes, J., Blome, C., et al. 2022, ApJL, 936, L14
Press, W. H., & Schechter, P. 1974, ApJ, 187, 425
Qin, Y., Duffy, A. R., Mutch, S. J., et al. 2019, MNRAS, 487, 1946
Regan, J. A., & Haehnelt, M. G. 2009a, MNRAS, 396, 343
Regan, J. A., & Haehnelt, M. G. 2009b, MNRAS, 393, 858
Reines, A. E., & Volonteri, M. 2015, ApJ, 813, 82
Scoggins, M. T., & Haiman, Z. 2024, MNRAS, 531, 4584
Scoggins, M. T., Haiman, Z., & Wise, J. H. 2023, MNRAS, 519, 2155
Somerville, R. S., & Davé, R. 2015, ARA&A, 53, 51
Stone, M. A., Lyu, J., Rieke, G. H., Alberts, S., & Hainline, K. N. 2024, ApJ, 964, 90
Tagawa, H., Haiman, Z., & Kocsis, B. 2020, ApJ, 898, 25
Taylor, A. J., Finkelstein, S. L., Kocevski, D. D., et al. 2024, arXiv:2409.06772
Trinca, A., Schneider, R., Valiante, R., et al. 2022, MNRAS, 511, 616
van den Bosch, R. C. E., Gebhardt, K., Gültekin, K., et al. 2012, Natur, 491, 729
Volonteri, M., Haardt, F., & Madau, P. 2003, ApJ, 582, 559
Volonteri, M., Habouzit, M., & Colpi, M. 2021, NatRP, 3, 732
Wadsley, J. W., Stadel, J., & Quinn, T. 2004, NewA, 9, 137
Wang, Y.-Y., Lei, L., Yuan, G.-W., & Fan, Y.-Z. 2023, ApJL, 954, L48
Weinberger, R., Springel, V., Hernquist, L., et al. 2017, MNRAS, 465, 3291
Wu, X.-B., Wang, F., Fan, X., et al. 2015, Natur, 518, 512
Wyithe, J. S. B., & Padmanabhan, T. 2006, MNRAS, 366, 1029
Yuan, F., & Narayan, R. 2014, ARA&A, 52, 529
Yue, M., Eilers, A.-C., Simcoe, R. A., et al. 2023, ApJ, 966, 176
Zhuang, M.-Y., & Ho, L. C. 2023, NatAs, 7, 1376